

# No Need For Real Anomaly: MLLM Empowered Zero-Shot Video Anomaly Detection

Zunkai Dai<sup>1</sup>, Ke Li<sup>1,†</sup>, Jiajia Liu<sup>2</sup>, Jie Yang<sup>1</sup>, Yuanyuan Qiao<sup>1,†</sup>

<sup>1</sup>Beijing University of Posts and Telecommunications

<sup>2</sup>Northwestern Polytechnical University

{daizk, like1990, janeyang, yyqiao}@bupt.edu.cn, liujiajia@nwpu.edu.cn

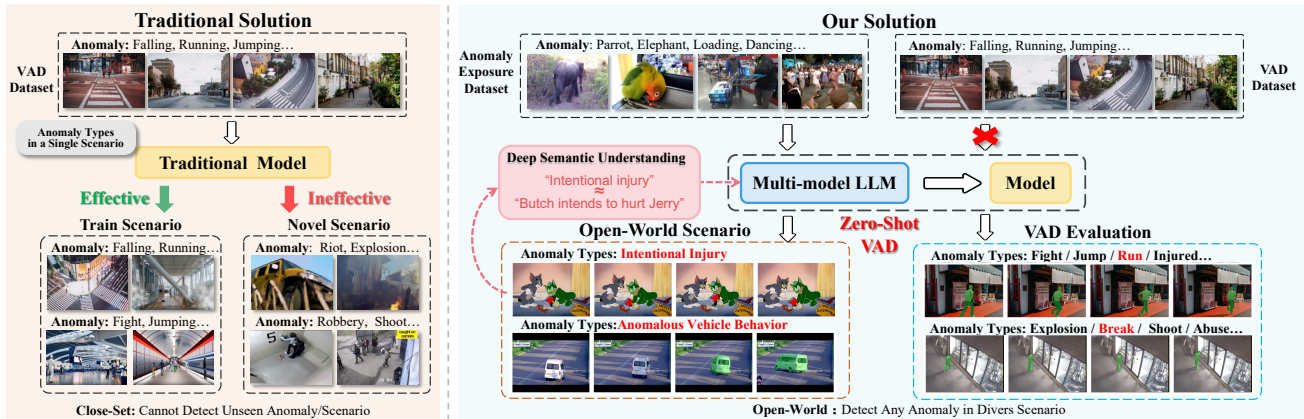


Fig. 1. **Motivation.** **Left:** Existing VAD methods rely on training with anomaly data from single scenarios, resulting in poor generalization capability to novel anomaly types or unseen scenarios. **Right:** Our LAVIDA model leverages MLLM to understand deep anomaly semantics, enabling generalization to arbitrary anomaly types across diverse scenarios. The training data consists of pseudo anomaly data synthesized from external datasets, without incorporating any VAD data.

## Abstract

The collection and detection of video anomaly data has long been a challenging problem due to its rare occurrence and spatio-temporal scarcity. Existing video anomaly detection (VAD) methods underperform in open-world scenarios. Key contributing factors include limited dataset diversity, and inadequate understanding of context-dependent anomalous semantics. To address these issues, i) we propose LAVIDA, an end-to-end zero-shot video anomaly detection framework. ii) LAVIDA employs an Anomaly Exposure Sampler that transforms segmented objects into pseudo-anomalies to enhance model adaptability to unseen anomaly categories. It further integrates a Multi-modal Large Language Model (MLLM) to bolster semantic comprehension capabilities. Additionally, iii) we design a token compression approach based on reverse attention to handle the spatio-temporal scarcity of anomalous patterns and decrease computational cost. The training

process is conducted solely on pseudo anomalies without any VAD data. Evaluations across four benchmark VAD datasets demonstrate that LAVIDA achieves SOTA performance in both frame-level and pixel-level anomaly detection under the zero-shot setting. Our code is available in <https://github.com/VitaminCreed/LAVIDA>.

## 1. Introduction

Video Anomaly Detection (VAD) aims to identify behaviors that deviate from normal patterns or represent unexpected events in video sequences. Classical VAD methods assume static scenes, closed-set anomaly categories, and stationary data distributions, yet these assumptions fail in dynamic environments where scenes evolve, behaviors shift, and distributions drift continuously. Recent works have reconceptualized VAD in open-world settings, where systems must detect unseen anomalies, operate without predefined taxonomies, and learn continuously. This capability is critical for safety-critical applications, enabling world models

<sup>†</sup>Corresponding author.

to perceive and adapt to unexpected events.

Recent open-set VAD [1, 8, 53] and open-vocabulary VAD [14, 34, 37] approaches have developed promising capabilities for detecting previously unseen anomaly types. However, single-scene training limits their generalization to unseen scenarios. Some methods [2, 27, 39, 47] leverage multimodal large language models (MLLMs) to obtain anomaly scores, achieving training-free detection. However, they heavily rely on frame-wise or clip-wise text outputs generated by MLLMs, which significantly limits their practical applicability.

Improving the generalization performance of VAD models faces three primary challenges: i) *Limited diversity in available anomaly datasets*: Existing VAD datasets contain limited scenarios and anomaly types, which restricts model learning capabilities and makes them inadequate for real open-world applications; ii) *Context-dependent semantic interpretations of anomalies*: Anomaly semantics vary according to different scenarios, while current methods lack sufficient semantic understanding, failing to comprehend unseen scenarios and novel anomaly types, and struggle to adapt detection targets dynamically; and iii) *Spatiotemporal sparsity of anomalies*: Anomalies often occupy minimal temporal or spatial regions. The abundance of redundant visual information significantly increases computational cost. Moreover, detection models struggle to effectively leverage the coarse-grained (video-level) contextual semantic features generated by MLLMs, thereby overlooking localized anomalous patterns in spatiotemporal dimensions.

To address these challenges, we propose LAVIDA (LLM-Assisted Video Anomaly Detection Approach), an end-to-end VAD framework that leverages MLLMs and requires no real VAD data during training. To overcome the limited diversity of anomalies in existing datasets, we design an Anomaly Exposure Sampler that transforms widely accessible semantic segmentation datasets that contain diverse semantics into pseudo anomalies, thereby expanding VAD scenarios and anomaly types while eliminating the dependence of training on VAD data. To enhance semantic understanding, we employ an MLLM-integrated semantic feature extractor to capture clip-level semantic representations, utilizing MLLMs’ open-world understanding to significantly improve anomaly semantic comprehension and resolve context-dependency challenges. To enable the model to focus on local anomaly patterns, considering the spatiotemporal sparsity of anomalies, we apply a reverse-attention-based token compression method that substantially reduces irrelevant background visual information, and leverage learnable query tokens that simultaneously access clip-level context and frame-level details. At the end, we execute comprehensive anomaly detection at both frame and pixel granularities.

LAVIDA demonstrates exceptional generalization capa-

bilities, achieving state-of-the-art performance in zero-shot detection scenarios. After training on the Anomaly Exposure datasets (external segmentation datasets), evaluations on four unseen datasets yield: 76.45% AUC on UBnormal, 85.28% AUC on ShanghaiTech, 82.18% AUC on UCF-Crime (outperforming unsupervised methods), 90.62% AP on XD-Violence (surpassing weakly-supervised methods), and 87.68% pixel-level AUC on UCSD Ped2 (current state-of-the-art pixel-level zero-shot performance).

In summary, our contributions are as follows:

- We propose an end-to-end zero-shot VAD framework, LAVIDA, which leverages MLLMs to extract video anomaly semantic representations and enables frame/pixel-level open-world anomaly detection.
- We introduce an Anomaly Exposure Sampler: a training strategy that repurposes segmentation targets as pseudo-anomalies, enabling training without VAD data and improving adaptability to diverse scenarios.
- We design a token compression method for LLM-based VAD model, which mitigates background interference and reduces computational costs for LLMs.
- Extensive experiments show that our method achieves state-of-the-art zero-shot performance, and achieves competitive results w.r.t. unsupervised VAD methods at the frame level, and competitive zero-shot performance at the pixel level.

## 2. Related Work

### 2.1. Traditional VAD Methods

Traditional video anomaly detection can be categorized into unsupervised and weakly-supervised approaches. Unsupervised methods assume that only normal samples exist in the training set and learn normal patterns through one-class classification (OCC) [25, 26, 31, 33, 44] or self-supervised tasks [5, 7, 16, 24, 40, 50]. Weakly-supervised VAD (WS-VAD) detects anomalies using only video-level annotations without requiring precise temporal or spatial localization [15, 28, 30, 32, 45]. Recent advances leverage pre-trained models and vision-language models to enhance detection performance [11, 19, 35, 41]. However, unsupervised methods struggle with unseen normal patterns and anomalous patterns similar to normal ones, and weakly-supervised methods can only recognize anomaly types present in the training set.

### 2.2. Open-World VAD Methods

To improve model generalization capabilities for unknown anomaly types, researchers have proposed open-set VAD and open-vocabulary VAD approaches. Open-set VAD was first introduced by AcSintoae et al. [1] with a benchmark dataset and evaluation framework. Subsequent approaches have explored evidential deep learning with normalizing

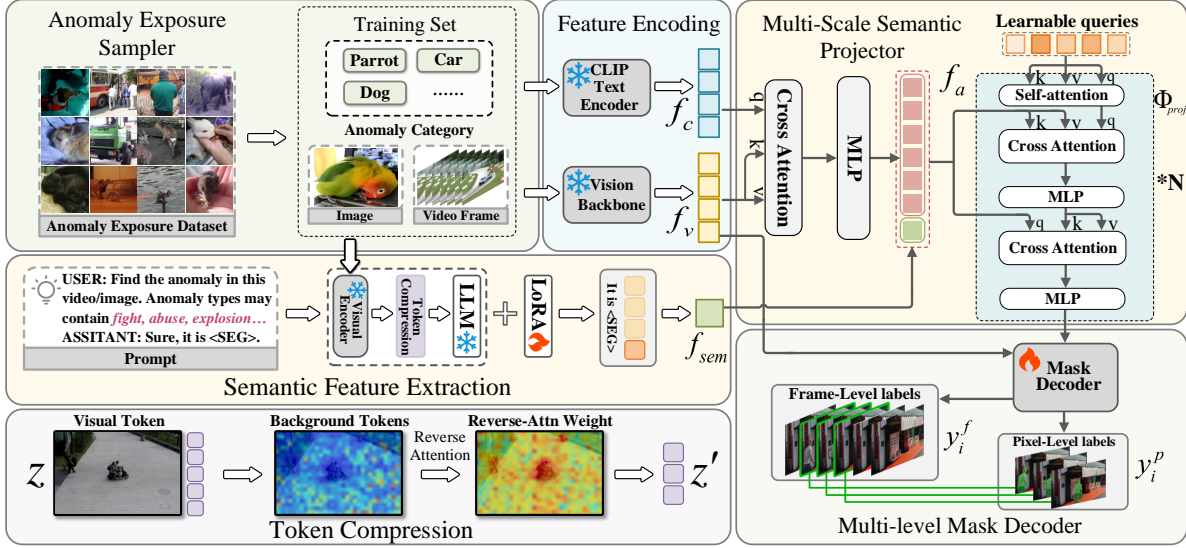


Fig. 2. **Overview of LAVIDA Framework.** LAVIDA is trained solely on a comprehensive Anomaly Exposure datasets, and consists of five key components: a MLLM, a text encoder, a vision backbone, a SAM2 mask decoder, and a Multi-scale Semantic Projector.

flows [53] and lightweight pose-based normalizing flows frameworks [8]. Open vocabulary VAD enhances anomaly categorization by leveraging vision-language models. Wu et al. [34] first introduce open-vocabulary video anomaly detection (OVVAD) using CLIP. Li et al. [14] leverages visual and textual information with label relations to reduce detection ambiguity. Xu et al. [37] uses learnable prompts and graph attention networks. Nevertheless, these methods remain restricted to particular scenarios and cannot adaptively adjust detection targets based on contextual changes, which prevents these methods from achieving truly open-world VAD capabilities.

### 2.3. LLM-based Video Anomaly Analysis

Current applications of MLLMs in Video Anomaly Detection (VAD) can be categorized into training-free VAD methods and Video Anomaly Understanding (VAU) approaches. Training-free VAD methods utilize MLLMs to analyze video clips or frames, extracting anomaly scores from the generated textual outputs. Zanella et al. [47] extract and refine anomaly scores from frame-wise textual outputs. Yang et al. [39] derive anomaly detection rules from training datasets for inference. Ahn et al. [2] employ CLIP to guide MLLMs toward anomalous regions for more accurate scoring. Shao et al. [27] integrate dynamic graphs to mine event boundaries, enabling MLLMs to focus on event intervals. Despite eliminating training requirements, these methods rely on frame-wise or clip-wise textual outputs, incurring high temporal costs and limiting prediction granularity to frame or clip level, thus preventing spatial localization of anomalies. On the other hand, VAU methods focus on the semantic understanding capabilities

of MLLMs to provide explanations for anomalies. Some studies [4, 29] construct interactive instruction data to deliver video-level anomaly explanations. Yuan et al. [43] refines VAU precision to the clip level. Zhang et al. [49] combines detection and understanding by outputting explanations for high-probability anomalous regions. Xing et al. [36] deploys audio data to enhance the understanding of anomalies. However, these methods prioritize using MLLMs for explanation generation while overlooking the intrinsic capability to detect unseen anomaly types.

## 3. Methods

### 3.1. Preliminary

The training dataset is an pseudo anomaly dataset  $\mathcal{D}_E = \{(x_i, y_i, c_i)\}_{i=1}^N$ , where  $x_i$  represents the input visual data encompassing both video and image modalities. For video samples,  $v_i \in \mathbb{R}^{T \times C \times H \times W}$  where  $T, C, H, W$  denote the number of frames, channels, height, and width, respectively, while for image samples,  $I_i \in \mathbb{R}^{C \times H \times W}$ . And  $c_i = \{c_{i,0}, c_{i,1}, \dots, c_{i,K-1}\}$  indicates the anomaly categories to be detected, and  $y_i = (y_i^f, y_i^p)$  denotes the corresponding anomaly labels with frame-level label  $y_i^f \in \{0, 1\}^T$  and pixel-level label  $y_i^p \in \{0, 1\}^{T \times H \times W}$ . During evaluation, the model is tested on unseen VAD datasets  $\mathcal{D}_{test} = \{(v_t, y_t, c_t)\}_{t=1}^M$ , where the anomaly categories  $c_t$  and video scenarios are different from the training dataset. Our objective is to predict  $y_t$  in  $\mathcal{D}_{test}$  under zero-shot conditions, where the test videos  $v_t$  and test anomaly categories  $c_t$  are not observed during training.

### 3.2. Overview

The LAVIDA framework comprises five key components, as illustrated in Fig. 2. First, an Anomaly Exposure Sampler reconstructs anomaly exposure dataset to form the training set. The input data then enters the Feature Encoding module, which encodes text, image, and video into feature vectors. Simultaneously, the Semantic Feature Extraction module encodes abnormal description prompts alongside vision data into a unified semantic feature via MLLM, with visual tokens being compressed by a token compression module. Thereafter, the Multi-Scale Semantic Projector fuses these semantic features with learnable query vectors and projects them into the mask decoder’s latent space. Ultimately, a Multi-Level Mask Decoder decodes these latent space features to output frame-level and pixel-level anomaly scores.

### 3.3. Anomaly Exposure Sampler

Visual semantic segmentation datasets provide rich scene diversity and comprehensive semantic categories. However, these datasets cannot be directly applied to VAD tasks, since anomalies occur rarely in datasets. To address this problem, we propose a two-step transformation of the anomaly exposure dataset, as illustrated in Fig. 3. We define the training dataset as  $\mathcal{D}_E = \{(x_i, y_i^p, s_i)\}_{i=1}^N$ , where  $s_i$  represents the text description of video clip  $v_i$ , and  $y_i^p$  represents pixel-level category labels. Our objective is to construct  $(c_i, y_i^f)$  for each sample, thereby transforming  $\mathcal{D}_E = \{(x_i, y_i^p, s_i)\}_{i=1}^N$  into  $\mathcal{D}_E = \{(x_i, y_i, c_i)\}_{i=1}^N$ .

For anomalous samples, only sparse anomaly events exist within the video. This means that  $c_i$  contains few content-relevant categories, with the majority being irrelevant. To construct  $c_i$  for each sample in  $\mathcal{D}_E$ , we introduce irrelevant categories from other samples within the same dataset, thereby requiring models to distinguish genuine anomaly categories from irrelevant ones. This can be represented as follows:

$$S_i^{irr} = \{s_j \mid j \sim \text{Unif}(\{1, \dots, n\} \setminus \{i\}), |J| = K_E - 1\} \quad (1)$$

where  $S_i^{irr}$  represents the set of irrelevant categories for the  $i$ -th sample, constructed by uniformly sampled from other samples in  $\mathcal{D}_E$ .  $K_E$  is the total number of categories. In practice,  $K_E$  is set as a random parameter to enable the MLLM to handle arbitrary numbers of anomaly types.

To model anomaly rarity, each sample is randomly labeled as normal (probability  $1 - p$ ) or anomaly (probability  $p$ ). For anomalous samples, the category set  $c_i$  combines genuine and irrelevant categories, with frame labels  $y_i^f$  set to positive. Normal samples contain only irrelevant categories and are assigned negative labels. Such an operation is demonstrated as,

$$(c_i, y_i^f) = \begin{cases} (S_i^{irr} \cup \{s_i\}, \mathbf{1}^T) & \text{with } p \\ (s_i, \mathbf{0}^T) & \text{with } 1 - p \end{cases} \quad (2)$$

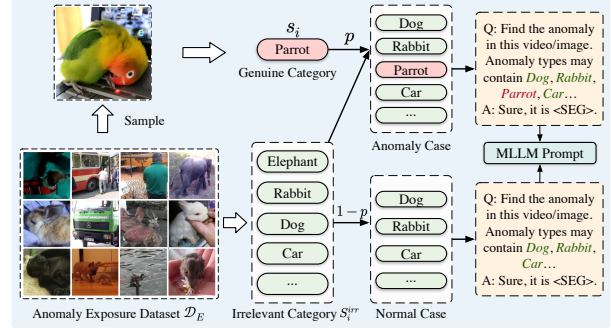


Fig. 3. **Anomaly Exposure Sampler:** We sample irrelevant categories from other samples to create anomaly categories, randomly designate samples as anomalous or normal based on probability.

where  $(c_i, y_i^f)$  denotes the output category set and frame-level labels for the  $i$ -th sample,  $T$  represents the total number of frames, and  $p$  controls the anomaly sampling probability.

### 3.4. Visual Token Compression

Anomaly objects typically constitute only a small fraction of visual data, while backgrounds constitute the vast majority. Excessive irrelevant background tokens degrade MLLM reasoning and incur substantial computational costs. We aim to deploy a training-free approach to compress background tokens while retaining anomaly-relevant features.

For VAD tasks, directly identifying anomalous tokens is difficult since the sparse spatial-temporal distribution of anomalous objects. However, background tokens are characterized by numerical predominance and high feature similarity, making them readily identifiable through density estimation. After visual encoding, the token features are represented as  $Z \in \mathbb{R}^{L_z \times D_z}$ , where  $L_z$  is the number of visual tokens and  $D_z$  is the token dimensionality. We compute the local density within the KNN neighborhood  $N_k(z_i)$  for each token  $z_i$  as:

$$\rho(z_i) = \frac{k}{\sum_{z_k \in N_k(z_i)} \|z_i - z_k\|^2} \quad (3)$$

We select the top- $L_r$  tokens with the highest density to form the background reference set  $Z^b \in \mathbb{R}^{L_r \times D_z}$ . To identify anomaly candidates, we employ a localized reverse attention mechanism [9]. Specifically, each token in  $Z$  is assigned to its nearest neighbor in  $Z^b$  based on the minimum Euclidean distance. For each background token  $Z_i^b$ , reverse attention is performed exclusively over its corresponding assigned tokens to highlight features most dissimilar to the background. This process is formulated as:

$$Z'_i = \text{Softmax} \left( -\frac{Z_i^b Z_{N_i}^T}{\sqrt{D_z}} \right) \cdot Z_{N_i} \quad (4)$$

where  $\mathcal{N}_i = \{j \mid \arg \min_k \|Z_j - Z_k^b\|_2 = i\}$  denotes the set of indices of tokens in  $Z$  that are closest to the  $i$ -th background token, and  $Z' \in \mathbb{R}^{L_r \times D_z}$  represents the aggregated anomalous features. This mechanism effectively compresses visual tokens into a compact  $L_r$ -length representation  $Z'$ .

### 3.5. Anomaly Semantics Extraction

Existing VAD methods are constrained by limited semantic comprehension capabilities, failing to understand anomalies in unseen scenarios. To address this limitation, we leverage MLLMs following previous work LISA [12] to extract rich anomaly semantic features that enable robust detection across diverse scenarios.

We extend the MLLM’s vocabulary with a special token  $\langle SEG \rangle$  to extract anomaly semantic features. Given a sample  $x_i$  the corresponding anomaly category  $c_i$ , we fill  $c_i$  into several predefined templates to construct the text prompt for the MLLM. For example: **USER:** *Find the anomaly in this video. Anomaly types may contain  $\{c_i\}$ .* **ASSISTANT:** *Sure, it is  $\langle SEG \rangle$ .* The  $\langle SEG \rangle$  token aggregates semantic information, and we extract its last-layer embedding as the anomaly semantic feature. Such an operation is demonstrated as:

$$f_{sem} = \Phi_{MLLM}(\mathbf{x}, \mathbf{c}) \quad (5)$$

where  $\Phi_{MLLM}$  is the MLLM,  $\mathbf{x}$  is the input samples,  $\mathbf{c}$  is the anomaly categories that are used to construct prompts, and  $f_{sem}$  is the extracted anomaly semantic feature.

### 3.6. Feature Encoding

For the input vision data  $x_i$  and anomaly categories  $c_i$ , we employ a vision backbone  $\Phi_v$  to extract visual features and a CLIP text encoder  $\Phi_t$  to extract textual features for anomaly categories:

$$f_v = \Phi_v(x_i), \quad f_c = \Phi_t(c_i) \quad (6)$$

where  $f_v \in \mathbb{R}^{T \times N_p \times D_v}$  represents vision feature.  $N_p$  denotes the number of patches within a single frame.  $f_c \in \mathbb{R}^{K \times D_t}$  represents anomaly category feature.

### 3.7. Multi-Scale Semantic Projector

While the MLLM effectively extracts semantic features for video anomalies, these representations remain at the video level without frame-specific granularity. To address this limitation, we propose a Multi-Scale Semantic Projector that integrates video-level semantic features with frame-level ones, generating frame-specific features  $f_{proj} \in \mathbb{R}^{T \times D_m}$  that are projected into the mask decoder to guide fine-grained detection in each frame.

To extract frame-level local anomaly information from the video sequence, we employ cross-attention mechanisms

between the anomaly category features and vision features, as demonstrated in the following formulation:

$$f_a = \mathbf{W}_o \cdot \text{CrossAttn}(\mathbf{W}_c f_c, W_v f_v, W_v f_v) \quad (7)$$

where  $f_v \in \mathbb{R}^{T \times L \times D_v}$  is vision features.  $\mathbf{W}_c \in \mathbb{R}^{D_c \times D_l}$ ,  $\mathbf{W}_v \in \mathbb{R}^{D_v \times D_l}$ , and  $\mathbf{W}_o \in \mathbb{R}^{D_l \times D_a}$  are learnable projection matrices.  $D_l$  and  $D_a$  represent the intermediate layer feature dimension of the output MLP and the hidden layer features of the multi-scale semantic projector, respectively.  $f_a \in \mathbb{R}^{T \times K \times D_a}$  is the output frame-level semantic features, containing the anomaly target information for each frame.

We expand  $f_{sem}$  along the temporal dimension and apply a mapping matrix  $W_{LLM}$ . Then we concatenate it with  $f_a$ . The combined features are projected into the latent space of the mask decoder via a Q-Former-like projector. Drawing inspiration from SAM, we formulate the projector as a two-way transformer architecture, as illustrated in Fig. 2, to facilitate the mutual updating of both learnable queries and the extracted features  $f_{sem}$  and  $f_a$ :

$$f_{proj} = \Phi_{proj}([W_{LLM} f_{sem}, f_a]) \quad (8)$$

where  $\Phi_{proj}$  is the projector and  $f_{proj} \in \mathbb{R}^{T \times D_m}$  represents the projected feature, and  $D_m$  is the latent dimension of Multi-Level Mask Decoder.

### 3.8. Multi-Level Mask Decoder

Existing VAD models typically focus on frame-level anomaly scores, limiting their detection granularity. To address this, our approach introduces a Multi-Level Mask Decoder initialized from SAM to enable both frame-level and pixel-level anomaly detection.

We feed  $f_{proj}$  as the sparse prompt embedding of SAM2. After integrating the visual features  $f_v$ , the mask decoder produces pixel-level scores and object score logits. The object score logits indicate the confidence of target object presence within the image or frame, which we leverage as the frame-level anomaly score. This process can be formulated as follows:

$$\hat{y}_i^f, \hat{y}_i^p = \Phi_d(f_{proj}, f_v) \quad (9)$$

where  $\hat{y}_i^f$  represents the frame-level score,  $\hat{y}_i^p$  denotes the pixel-level score, and  $\Phi_d$  is the mask decoder of SAM2.

### 3.9. Objective Function

The objective function comprises two components:  $\mathcal{L}_{txt}$  and  $\mathcal{L}_{seg}$ .

$$\mathcal{L} = \lambda_{txt} \mathcal{L}_{txt} + \lambda_{seg} \mathcal{L}_{seg} \quad (10)$$

where  $\lambda_{txt}$  and  $\lambda_{seg}$  are loss weight,  $\mathcal{L}_{txt}$  represents the text generation loss of the MLLM, and  $\mathcal{L}_{seg}$  denotes the

Methods	Venue	Training	UBnormal AUC (%)	ShanghaiTech AUC (%)	UCF-Crime AUC (%)	XD-Violence AP (%)
MemAE [6]	ICCV'19	Unsupervised	-	71.2	-	-
GODS [31]	ICCV'19	Unsupervised	-	-	70.4	61.56
MSMA [18]	ICLR'21	Unsupervised	-	76.7	64.5	-
GCL [46]	CVPR'22	Unsupervised	-	79.62	74.2	-
FastAno [23]	WACV'22	Unsupervised	-	72.2	-	-
FPDM [38]	ICCV'23	Unsupervised	62.7	78.6	74.7	-
MULDE [21]	CVPR'24	Unsupervised	72.8	81.3	78.5	-
AED-MAE [24]	CVPR'24	Unsupervised	58.5	79.1	-	-
MA-PDM [51]	AAAI'25	Unsupervised	63.4	79.2	-	-
CLIP-TSA [11]	ICIP'23	Weakly-Supervised	-	-	87.58	82.19
TPWNG [41]	CVPR'24	Weakly-Supervised	-	-	87.79	83.68
VadCLIP [35]	AAAI'24	Weakly-Supervised	-	-	<b>88.02</b>	84.51
Holmes-VAU [49]	CVPR'25	Weakly-Supervised	-	-	87.68	88.96
VERA [42]	CVPR'25	Weakly-Supervised	-	-	86.55	56.27
PI-VAD [20]	CVPR'25	Weakly-Supervised	-	-	90.33	85.37
Anomize [13]	CVPR'25	Weakly-Supervised	-	-	84.49	69.31
AnomalyRuler [39]	ECCV'24	Few-Shot	71.9	85.2	-	-
LAVAD [47]	CVPR'24	Zero-Shot	-	-	80.82	62.01
AnyAnomaly [2]	WACV'26	Zero-Shot	74.5	79.7	80.7	-
EventVAD [27]	ACM'25	Zero-Shot	-	-	82.03	64.04
<b>Ours</b>	-	Zero-Shot	<b>76.45</b>	<b>85.28</b>	82.18	<b>90.62</b>

Tab. 1. **Frame-level zero-shot performance compared with state-of-the-art methods.** We utilize AUC as the evaluation metric for UBnormal, ShanghaiTech and UCF-Crime datasets, and AP for the XD-Violence dataset. The best results are highlighted in bold.

anomaly detection loss that encompasses both frame-level and pixel-level performance enhancement. To facilitate optimization, we adopt SAM2’s training loss for  $\mathcal{L}_{seg}$ .

## 4. Experiment

Our training dataset includes a diverse collection of segmentation datasets without any VAD datasets. Detailed information regarding datasets, configurations, and additional results can be found in the supplementary material.

### 4.1. Qualitative Results

#### 4.1.1. Frame-Level Zero-Shot Evaluation

In Tab. 1, we present a comprehensive comparison of our proposed method against other SOTA approaches under zero-shot conditions across the UBnormal, ShanghaiTech, UCF-Crime, and XD-Violence datasets. The compared methods encompass four categories: unsupervised methods, weakly-supervised methods, few-shot methods, and zero-shot methods.

The experimental results demonstrate that our method attains 76.45%, 85.28% and 82.18% on the UBnormal, ShanghaiTech and UCF-Crime datasets, surpassing SOTA unsupervised, zero-shot and few-shot methods. On the XD-Violence dataset, our approach achieves 90.62%, outperforming SOTA methods. These datasets vary in both scenar-

ios and anomaly types. This superior performance demonstrates the effectiveness of our proposed method in handling both unseen scenarios and novel anomaly categories.

Our method does not surpass weakly-supervised approaches on UCF-Crime, which we attribute to the limitations of existing MLLMs in comprehending low-resolution videos. In contrast, UBnormal, ShanghaiTech, and XD-Violence are high-resolution datasets, where small abnormal targets remain distinguishable.

#### 4.1.2. Pixel-Level Zero-Shot Evaluation

We evaluate the zero-shot pixel-level performance of our method against SOTA approaches on the UCSD Ped2 dataset, as presented in Tab. 2. Our method achieves a pixel-level AUC of 87.68%, which represents a substantial improvement of 12.57% over the current SOTA method. This significant enhancement demonstrates that our approach possesses strong zero-shot anomaly localization capability in the spatial dimension.

### 4.2. Quantitative Results

Fig. 4 presents quantitative results for anomaly detection across six representative cases from different VAD datasets. For each case, the lower row displays frame-level anomaly scores over time with anomalous intervals highlighted in pink, and the upper row shows pixel-level detection results

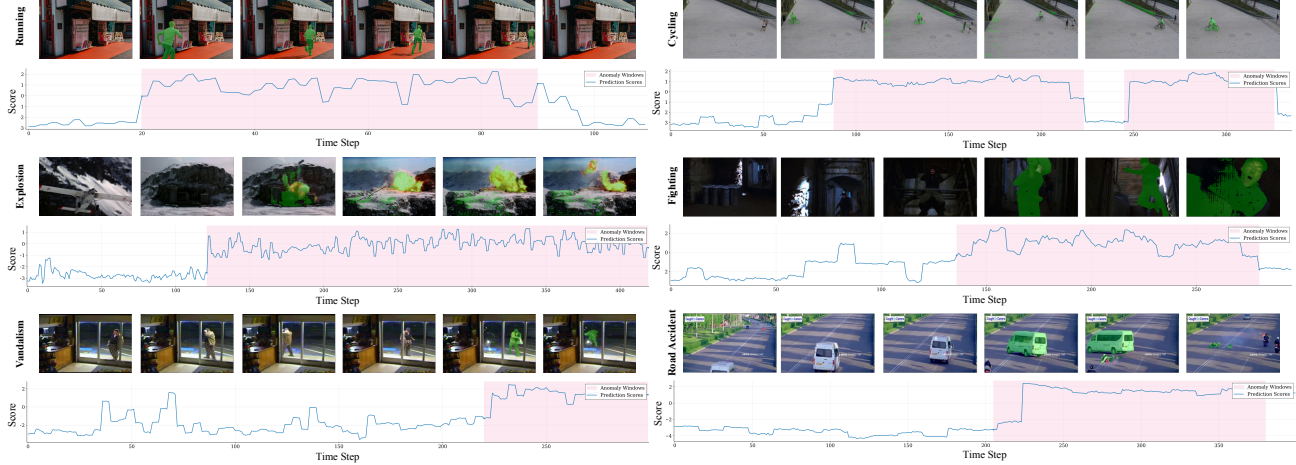


Fig. 4. **Qualitative Results for Anomaly Detection.** For each case, the first row presents pixel-level detection results which are masked by green. The second row displays frame-level anomaly scores, with temporal intervals of anomalous events marked in pink.

Method	Training	AUC(%)
AdaCLIP [3]	Finetune	53.06
AnomalyCLIP [52]	Finetune	54.25
DDAD [22]	Supervised.	55.87
SimpleNet [17]	Supervised	52.49
DRAEM [48]	Supervised	69.58
TAO [10]	Finetune	75.11
<b>Proposed</b>	<b>Zero-Shot</b>	<b>87.68</b>

Tab. 2. Pixel-level performance on UCSD Ped2.



Fig. 5. **Quantitative Visualizations for Open-World Scenarios.** The left panel shows the original image, and the right panel highlights detected anomalies with green masks.

at corresponding time steps with anomaly targets masked in green. Higher scores in pink regions and lower scores elsewhere demonstrate effective frame-level detection. Results show our model accurately identifies anomalous frames in unseen scenarios and generates precise pixel-level scores that delineate anomaly boundaries.

Fig. 5 presents open-world detection results. For each

case, the target anomaly category is specified in the text. The left panel shows original images, while the right panel presents detection results with anomalies highlighted in green. Our method demonstrates robust performance and strong reasoning capabilities in identifying arbitrary anomaly types across diverse scenarios.

### 4.3. Ablation Studies

#### 4.3.1. Analysis of the Anomaly Exposure Sampler

$\max(K_E)$	ShanghaiTech AUC (%)	UCF-Crime AUC (%)	XD-Violence AP (%)
10	73.34	67.11	55.44
20	80.13	80.02	91.20
30	85.02	82.06	90.30
40	76.41	77.93	75.32

Tab. 3. **Effect of the number of anomaly categories introduced in the anomaly exposure dataset.**

Tab. 3 shows the effect of anomaly category count  $K_E$  in the anomaly exposure dataset. To enable MLLMs to comprehend arbitrary anomaly types, we set  $K_E$  as a random variable and evaluate the impact by controlling  $\max(K_E)$ . Results show that performance is poor when  $\max(K_E) = 10$ , improves as the value increases, and reaches optimum around 30. Further increases beyond 30 cause performance degradation, which we attribute to excessively lengthy prompts that reduce the model’s focus on individual anomaly types.

#### 4.3.2. Analysis of Token Compression

Fig. 6 illustrates the token compression process. We leverage local density to identify tokens with the highest density values, which correspond closely to the background regions. During the reverse attention stage, tokens whose features are highly dissimilar to the background tokens are

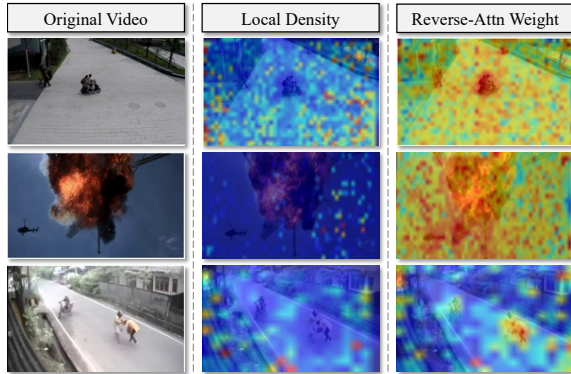
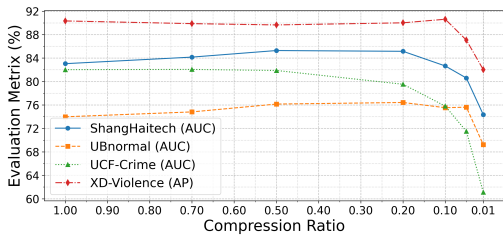
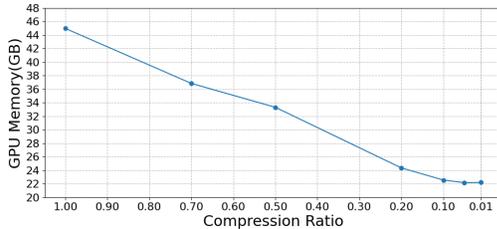


Fig. 6. **Token Compression Process.** The first column shows the original video frames. The second column shows local density, and the third shows reverse attention weights. Warmer colors indicate higher values.



(a) Compression ratio vs. model performance.



(b) Compression ratio vs. GPU memory usage.

Fig. 7. **Impression of compression ratio.** We normalize the frame size across all datasets to ensure a consistent number of total visual tokens. GPU memory usage is recorded during inference stage.

aggregated via reverse attention weight. As shown in the third column of Fig. 6, the reverse attention weights concentrate on regions that exhibit substantial dissimilarity from the background, which are typically anomaly-prone areas.

Fig. 7a presents the variation of performance across datasets with respect to the token compression ratio. For compression ratios above 0.1, performance remains relatively stable, demonstrating effective background token reduction without compromising model capability. On high-resolution datasets (UBnormal, ShanghaiTech, XD-Violence), we observe slight improvements, as background suppression enables better focus on small anomaly targets. When the compression ratio drops below 0.1, a marked performance degradation occurs due to substantial information

Adapter	frame-level			pixel-level
	ShanghaiTech AUC (%)	UCF-Crime AUC (%)	XD-Violence AP (%)	Ped2 AUC (%)
MLP	81.99	79.90	86.09	77.09
Q-Former	82.63	75.54	83.93	71.85
Proposed	85.28	82.06	90.62	87.68

Tab. 4. **Comparison among different adapters.**

number of queries	ShanghaiTech AUC (%)	UCF-Crime AUC (%)	XD-Violence AP (%)
24	58.85	66.63	50.14
32	77.41	77.96	88.31
48	80.64	80.06	90.30
64	77.96	67.11	89.15

Tab. 5. **Effect of the number of learnable queries.**

loss caused by excessive compression. UCF-Crime’s resolution is much lower than other datasets, making it the most susceptible to the visual compression.

Fig. 7b shows the corresponding GPU memory utilization versus the compression ratio. As the number of input visual tokens decreases, GPU memory consumption exhibits a linear reduction. At a compression ratio of 0.2, GPU memory usage is reduced to 54.1% of the baseline, with no substantial performance loss (UBNormal: +2.44%, ShanghaiTech: +2.24%, XD-Violence: -0.32%, UCF-Crime: -2.49%, Average: +0.47%).

### 4.3.3. Analysis of the Multi-Scale Semantic Projector

To validate the effectiveness of our Multi-Scale Semantic Projector, we compared it against MLP and Q-Former at both frame-level and pixel-level. The experimental results are presented in Tab. 4. The improvements at frame-level demonstrate the capability to capture temporal anomaly cues, while the enhancements at pixel-level indicate the ability to detect spatially sparse anomalies.

Tab. 5 presents the effect of learnable query count on zero-shot detection performance. With 24 queries, the model achieves suboptimal results due to limited representational capacity. Performance improves as query count increases, reaching a peak before declining when queries become excessive, causing convergence difficulties.

## 5. Conclusion

In this paper, we propose LAVIDA, an end-to-end zero-shot VAD approach that leverages MLLM and token compression algorithm to extract semantic anomaly features and an anomaly exposure sampler to enable anomaly detection in open-world scenarios without training VAD data. Multi-scale semantic projector is employed to extract hierarchical cues for joint frame- and pixel-level prediction. Extensive experiments the effectiveness across multiple benchmarks. We hope our work inspires further researches in developing open-world video anomaly detection and understanding.

**Acknowledgement.** This work is supported by the National Natural Science Foundation of China (No. 62272057).

## References

- [1] Andra Acsintoae, Andrei Florescu, Mariana-Iuliana Georgescu, Tudor Mare, Paul Sumedrea, Radu Tudor Ionescu, Fahad Shahbaz Khan, and Mubarak Shah. Ub-normal: New benchmark for supervised open-set video anomaly detection. In *Proceedings of the IEEE/CVF conference on computer vision and pattern recognition*, pages 20143–20153, 2022. 2
- [2] Sunghyun Ahn, Youngwan Jo, Kijung Lee, Sein Kwon, Inpyo Hong, and Sanghyun Park. Anyanomaly: Zero-shot customizable video anomaly detection with lvlm. *arXiv preprint arXiv:2503.04504*, 2025. 2, 3, 6
- [3] Yunkang Cao, Jiangning Zhang, Luca Frittoli, Yuqi Cheng, Weiming Shen, and Giacomo Boracchi. Adaclip: Adapting clip with hybrid learnable prompts for zero-shot anomaly detection. In *European Conference on Computer Vision*, pages 55–72. Springer, 2024. 7
- [4] Hang Du, Sicheng Zhang, Binzhu Xie, Guoshun Nan, Jiayang Zhang, Junrui Xu, Hangyu Liu, Sicong Leng, Jiangming Liu, Hehe Fan, et al. Uncovering what why and how: A comprehensive benchmark for causation understanding of video anomaly. In *Proceedings of the IEEE/CVF Conference on Computer Vision and Pattern Recognition*, pages 18793–18803, 2024. 3
- [5] Xinyang Feng, Dongjin Song, Yuncong Chen, Zhengzhang Chen, Jingchao Ni, and Haifeng Chen. Convolutional transformer based dual discriminator generative adversarial networks for video anomaly detection. In *Proceedings of the 29th ACM international conference on multimedia*, pages 5546–5554, 2021. 2
- [6] Dong Gong, Lingqiao Liu, Vuong Le, Budhaditya Saha, Moussa Reda Mansour, Svetha Venkatesh, and Anton van den Hengel. Memorizing normality to detect anomaly: Memory-augmented deep autoencoder for unsupervised anomaly detection, 2019. 6
- [7] Yi Hao, Jie Li, Nannan Wang, Xiaoyu Wang, and Xinbo Gao. Spatiotemporal consistency-enhanced network for video anomaly detection. *Pattern Recognition*, 121:108232, 2022. 2
- [8] Or Hirschorn and Shai Avidan. Normalizing flows for human pose anomaly detection. In *Proceedings of the IEEE/CVF International Conference on Computer Vision*, pages 13545–13554, 2023. 2, 3
- [9] Qin Huang, Chunyang Xia, Chihao Wu, Siyang Li, Ye Wang, Yuhang Song, and C. C. Jay Kuo. Semantic segmentation with reverse attention, 2017. 4
- [10] Yuzhi Huang, Chenxin Li, Haitao Zhang, Zixu Lin, Yunlong Lin, Hengyu Liu, Wuyang Li, Xinyu Liu, Jiechao Gao, Yue Huang, et al. Track any anomalous object: A granular video anomaly detection pipeline. In *Proceedings of the Computer Vision and Pattern Recognition Conference*, pages 8689–8699, 2025. 7
- [11] Hyekang Kevin Joo, Khoa Vo, Kashu Yamazaki, and Ngan Le. Clip-tsa: Clip-assisted temporal self-attention for weakly-supervised video anomaly detection. In *2023 IEEE International Conference on Image Processing (ICIP)*, pages 3230–3234. IEEE, 2023. 2, 6
- [12] Xin Lai, Zhuotao Tian, Yukang Chen, Yanwei Li, Yuhui Yuan, Shu Liu, and Jiaya Jia. Lisa: Reasoning segmentation via large language model. *arXiv preprint arXiv:2308.00692*, 2023. 5
- [13] Fei Li, Wenxuan Liu, Jingjing Chen, Ruixu Zhang, Yuran Wang, Xian Zhong, and Zheng Wang. Anomize: Better open vocabulary video anomaly detection. In *Proceedings of the IEEE/CVF Conference on Computer Vision and Pattern Recognition (CVPR)*, pages 29203–29212, 2025. 6
- [14] Fei Li, Wenxuan Liu, Jingjing Chen, Ruixu Zhang, Yuran Wang, Xian Zhong, and Zheng Wang. Anomize: Better open vocabulary video anomaly detection. In *Proceedings of the Computer Vision and Pattern Recognition Conference*, pages 29203–29212, 2025. 2, 3
- [15] Shuo Li, Fang Liu, and Licheng Jiao. Self-training multi-sequence learning with transformer for weakly supervised video anomaly detection. In *Proceedings of the AAAI Conference on Artificial Intelligence*, pages 1395–1403, 2022. 2
- [16] Zhian Liu, Yongwei Nie, Chengjiang Long, Qing Zhang, and Guiqing Li. A hybrid video anomaly detection framework via memory-augmented flow reconstruction and flow-guided frame prediction. In *Proceedings of the IEEE/CVF international conference on computer vision*, pages 13588–13597, 2021. 2
- [17] Zhikang Liu, Yiming Zhou, Yuansheng Xu, and Zilei Wang. Simplenet: A simple network for image anomaly detection and localization. In *Proceedings of the IEEE/CVF conference on computer vision and pattern recognition*, pages 20402–20411, 2023. 7
- [18] Ahsan Mahmood, Junier Oliva, and Martin Styner. Multi-scale score matching for out-of-distribution detection. *arXiv preprint arXiv:2010.13132*, 2020. 6
- [19] Snehashis Majhi, Giacomo D’Amicantonio, Antitza Dantcheva, Quan Kong, Lorenzo Garattoni, Gianpiero Francesca, Egor Bondarev, and Francois Bremond. Just dance with pi! a poly-modal inductor for weakly-supervised video anomaly detection. In *Proceedings of the Computer Vision and Pattern Recognition Conference (CVPR)*, pages 24265–24274, 2025. 2
- [20] Snehashis Majhi, Giacomo D’Amicantonio, Antitza Dantcheva, Quan Kong, Lorenzo Garattoni, Gianpiero Francesca, Egor Bondarev, and François Brémond. Just dance with pi! a poly-modal inductor for weakly-supervised video anomaly detection. In *Proceedings of the Computer Vision and Pattern Recognition Conference*, pages 24265–24274, 2025. 6
- [21] Jakub Micorek, Horst Possegger, Dominik Narnhofer, Horst Bischof, and Mateusz Kozinski. Mulde: Multiscale log-density estimation via denoising score matching for video anomaly detection. In *Proceedings of the IEEE/CVF Conference on Computer Vision and Pattern Recognition*, pages 18868–18877, 2024. 6

- [22] Arian Mousakhan, Thomas Brox, and Jawad Tayyub. Anomaly detection with conditioned denoising diffusion models. In *DAGM German Conference on Pattern Recognition*, pages 181–195. Springer, 2024. 7
- [23] Chaewon Park, MyeongAh Cho, Minhyeok Lee, and Sangyoun Lee. Fastano: Fast anomaly detection via spatio-temporal patch transformation. In *Proceedings of the IEEE/CVF Winter Conference on Applications of Computer Vision*, pages 2249–2259, 2022. 6
- [24] Nicolae-C Ristea, Florinel-Alin Croitoru, Radu Tudor Ionescu, Marius Popescu, Fahad Shahbaz Khan, Mubarak Shah, et al. Self-distilled masked auto-encoders are efficient video anomaly detectors. In *Proceedings of the IEEE/CVF conference on computer vision and pattern recognition*, pages 15984–15995, 2024. 2, 6
- [25] Mohammad Sabokrou, Mohammad Khalooei, Mahmood Fathy, and Ehsan Adeli. Adversarially learned one-class classifier for novelty detection. In *Proceedings of the IEEE conference on computer vision and pattern recognition*, pages 3379–3388, 2018. 2
- [26] Bernhard Schölkopf, Robert C Williamson, Alex Smola, John Shawe-Taylor, and John Platt. Support vector method for novelty detection. *Advances in neural information processing systems*, 12, 1999. 2
- [27] Yihua Shao, Haojin He, Sijie Li, Siyu Chen, Xinwei Long, Fanhu Zeng, Yuxuan Fan, Muyang Zhang, Ziyang Yan, Ao Ma, et al. Eventvad: Training-free event-aware video anomaly detection. *arXiv preprint arXiv:2504.13092*, 2025. 2, 3, 6
- [28] Waqas Sultani, Chen Chen, and Mubarak Shah. Real-world anomaly detection in surveillance videos. In *Proceedings of the IEEE conference on computer vision and pattern recognition*, pages 6479–6488, 2018. 2
- [29] Jiaqi Tang, Hao Lu, Ruizheng Wu, Xiaogang Xu, Ke Ma, Cheng Fang, Bin Guo, Jiangbo Lu, Qifeng Chen, and Yingcong Chen. Hawk: Learning to understand open-world video anomalies. *Advances in Neural Information Processing Systems*, 37:139751–139785, 2024. 3
- [30] Yu Tian, Guansong Pang, Yuanhong Chen, Rajvinder Singh, Johan W Verjans, and Gustavo Carneiro. Weakly-supervised video anomaly detection with robust temporal feature magnitude learning. In *Proceedings of the IEEE/CVF international conference on computer vision*, pages 4975–4986, 2021. 2
- [31] Jue Wang and Anoop Cherian. Gods: Generalized one-class discriminative subspaces for anomaly detection. In *Proceedings of the IEEE/CVF International Conference on Computer Vision*, pages 8201–8211, 2019. 2, 6
- [32] Peng Wu and Jing Liu. Learning causal temporal relation and feature discrimination for anomaly detection. *IEEE Transactions on Image Processing*, 30:3513–3527, 2021. 2
- [33] Peng Wu, Jing Liu, and Fang Shen. A deep one-class neural network for anomalous event detection in complex scenes. *IEEE transactions on neural networks and learning systems*, 31(7):2609–2622, 2019. 2
- [34] Peng Wu, Xuerong Zhou, Guansong Pang, Yujia Sun, Jing Liu, Peng Wang, and Yanning Zhang. Open-vocabulary video anomaly detection. In *Proceedings of the IEEE/CVF Conference on Computer Vision and Pattern Recognition*, pages 18297–18307, 2024. 2, 3
- [35] Peng Wu, Xuerong Zhou, Guansong Pang, Lingru Zhou, Qingsen Yan, Peng Wang, and Yanning Zhang. Vadclip: Adapting vision-language models for weakly supervised video anomaly detection. In *Proceedings of the AAAI Conference on Artificial Intelligence*, pages 6074–6082, 2024. 2, 6
- [36] Zhenghao Xing, Hao Chen, Binzhu Xie, Jiaqi Xu, Ziyu Guo, Xuemiao Xu, Jianye Hao, Chi-Wing Fu, Xiaowei Hu, and Pheng-Ann Heng. Echotraffic: Enhancing traffic anomaly understanding with audio-visual insights. In *Proceedings of the Computer Vision and Pattern Recognition Conference (CVPR)*, pages 19098–19108, 2025. 3
- [37] Chenting Xu, Ke Xu, Xinghao Jiang, and Tanfeng Sun. Plovad: Prompting vision-language models for open vocabulary video anomaly detection. *IEEE Transactions on Circuits and Systems for Video Technology*, 2025. 2, 3
- [38] Cheng Yan, Shiyu Zhang, Yang Liu, Guansong Pang, and Wenjun Wang. Feature prediction diffusion model for video anomaly detection. In *Proceedings of the IEEE/CVF international conference on computer vision*, pages 5527–5537, 2023. 6
- [39] Yuchen Yang, Kwonjoon Lee, Behzad Dariush, Yinzhi Cao, and Shao-Yuan Lo. Follow the rules: Reasoning for video anomaly detection with large language models. In *European Conference on Computer Vision*, pages 304–322. Springer, 2024. 2, 3, 6
- [40] Zhiwei Yang, Jing Liu, Zhaoyang Wu, Peng Wu, and Xiaotao Liu. Video event restoration based on keyframes for video anomaly detection. In *Proceedings of the IEEE/CVF conference on computer vision and pattern recognition*, pages 14592–14601, 2023. 2
- [41] Zhiwei Yang, Jing Liu, and Peng Wu. Text prompt with normality guidance for weakly supervised video anomaly detection. In *Proceedings of the IEEE/CVF conference on computer vision and pattern recognition*, pages 18899–18908, 2024. 2, 6
- [42] Muchao Ye, Weiyang Liu, and Pan He. Vera: Explainable video anomaly detection via verbalized learning of vision-language models, 2024. 6
- [43] Tongtong Yuan, Xuange Zhang, Kun Liu, Bo Liu, Chen Chen, Jian Jin, and Zhenzhen Jiao. Towards surveillance video-and-language understanding: New dataset baselines and challenges. In *Proceedings of the IEEE/CVF conference on computer vision and pattern recognition*, pages 22052–22061, 2024. 3
- [44] Muhammad Zaigham Zaheer, Jin-ha Lee, Marcella Astrid, and Seung-Ik Lee. Old is gold: Redefining the adversarially learned one-class classifier training paradigm. In *Proceedings of the IEEE/CVF conference on computer vision and pattern recognition*, pages 14183–14193, 2020. 2
- [45] Muhammad Zaigham Zaheer, Arif Mahmood, Marcella Astrid, and Seung-Ik Lee. Claws: Clustering assisted weakly supervised learning with normalcy suppression for anomalous event detection. In *European Conference on Computer Vision*, pages 358–376. Springer, 2020. 2

- [46] M Zaigham Zaheer, Arif Mahmood, M Haris Khan, Mattia Segu, Fisher Yu, and Seung-Ik Lee. Generative cooperative learning for unsupervised video anomaly detection. In *Proceedings of the IEEE/CVF conference on computer vision and pattern recognition*, pages 14744–14754, 2022. [6](#)
- [47] Luca Zanella, Willi Menapace, Massimiliano Mancini, Yiming Wang, and Elisa Ricci. Harnessing large language models for training-free video anomaly detection. In *Proceedings of the IEEE/CVF Conference on Computer Vision and Pattern Recognition*, pages 18527–18536, 2024. [2](#), [3](#), [6](#)
- [48] Vitjan Zavrtnik, Matej Kristan, and Danijel Skočaj. Draem—a discriminatively trained reconstruction embedding for surface anomaly detection. In *Proceedings of the IEEE/CVF international conference on computer vision*, pages 8330–8339, 2021. [7](#)
- [49] Huaxin Zhang, Xiaohao Xu, Xiang Wang, Jialong Zuo, Xiaonan Huang, Changxin Gao, Shanjun Zhang, Li Yu, and Nong Sang. Holmes-vau: Towards long-term video anomaly understanding at any granularity. In *Proceedings of the Computer Vision and Pattern Recognition Conference (CVPR)*, pages 13843–13853, 2025. [3](#), [6](#)
- [50] Yuanhong Zhong, Xia Chen, Jinyang Jiang, and Fan Ren. A cascade reconstruction model with generalization ability evaluation for anomaly detection in videos. *Pattern Recognition*, 122:108336, 2022. [2](#)
- [51] Hang Zhou, Jiale Cai, Yuteng Ye, Yonghui Feng, Chenxing Gao, Junqing Yu, Zikai Song, and Wei Yang. Video anomaly detection with motion and appearance guided patch diffusion model. In *Proceedings of the AAAI Conference on Artificial Intelligence*, pages 10761–10769, 2025. [6](#)
- [52] Qihang Zhou, Guansong Pang, Yu Tian, Shibo He, and Jiming Chen. Anomalyclip: Object-agnostic prompt learning for zero-shot anomaly detection. *arXiv preprint arXiv:2310.18961*, 2023. [7](#)
- [53] Yuansheng Zhu, Wentao Bao, and Qi Yu. Towards open set video anomaly detection. In *European Conference on Computer Vision*, pages 395–412. Springer, 2022. [2](#), [3](#)